Gauge–Uzawa methods for incompressible flows with variable density

Jae-Hong Pyo [a,1], Jie Shen [b,*,2]

[a] *Department of Mathematics, Yonsei University, Seoul, South Korea*
[b] *Department of Mathematics, Purdue University, 150 N University Street, West Lafayette, IN 47907, USA*

Abstract

Two new Gauge–Uzawa schemes are constructed for incompressible flows with variable density. One is in the conserved form while the other is in the convective form. It is shown that the first-order versions of both schemes, in their semi-discretized form, are unconditionally stable. Numerical experiments indicate that the first-order (resp. second-order) versions of the two schemes lead to first-order (resp. second-order) convergence rate for all variables and that these schemes are suitable for handling problems with large density ratios such as in the situation of air bubble rising in water.
© 2006 Elsevier Inc. All rights reserved.

MSC: 65M12; 65M60; 76D05

Keywords: Incompressible flows with variable density; Projection methods; Gauge–Uzawa method; Finite element method; Stability

1. Introduction

We consider in this paper numerical approximations of incompressible viscous flows with variable density governed by the following coupled nonlinear system:

$$\rho_t + \mathbf{u} \cdot \nabla \rho = 0, \tag{1.1a}$$
$$\rho(\mathbf{u}_t + (\mathbf{u} \cdot \nabla)\mathbf{u}) + \nabla p - \mu \Delta \mathbf{u} = \mathbf{f} \quad \text{in } \Omega \times (0, T], \tag{1.1b}$$
$$\nabla \cdot \mathbf{u} = 0, \tag{1.1c}$$

---

where the unknowns are the density $\rho > 0$, the velocity field $\mathbf{u}$ and the pressure p; μ is the dynamic viscosity coefficient, $\mathbf{f}$ represents the external force, Ω is a bounded domain in $\mathbb{R}^d$ ($d = 2$ or 3) and $T > 0$ is fixed time. The system (1.1) is supplemented with initial and boundary conditions for $\mathbf{u}$ and ρ:

$$\begin{cases} \rho(\mathbf{x}, 0) = \rho_0(\mathbf{x}) & \text{in } \Omega \text{ and } \rho(\mathbf{x}, t)|_{\Gamma_{\mathbf{u}(\mathbf{x},t)}} = r(\mathbf{x}, t), \\ \mathbf{u}(\mathbf{x}, 0) = \mathbf{u}_0(\mathbf{x}) & \text{in } \Omega \text{ and } \mathbf{u}(\mathbf{x}, t)|_{\Gamma} = \mathbf{g}(\mathbf{x}, t), \end{cases} \tag{1.2}$$

where $\Gamma = \partial\Omega$, and for any velocity field $\mathbf{v}$, $\Gamma_{\mathbf{v}}$ is the inflow boundary defined by

$$\Gamma_{\mathbf{v}} := \{\mathbf{x} \in \Gamma : \mathbf{v}(\mathbf{x}) \cdot \mathbf{v} < 0\}$$

with $\mathbf{v}$ being the outward unit normal vector. We note that no initial and boundary condition is needed for the pressure p which can be viewed as a Lagrange multiplier whose mathematical role is to enforce the incompressibility condition (1.1c). We refer to [9] for the mathematical theory on the well posedness of (1.1)–(1.2).

How to construct stable and efficient numerical schemes for the system (1.1)–(1.2) is challenging since, in addition to all the difficulties associated with the incompressible flows with constant density, it involves a transport equation for the density ρ which enforces, in addition to the incompressibility, that the mass density remains unchanged during the fluid motion. It is now well established (see, for instance, the review [5] and the references therein) that the difficulties associated with the incompressibility can be effectively handled by using a suitable projection type scheme originally proposed by Chorin [2] and Temam [14]. This approach has been used in [1,6,8], among others, for incompressible flows with variable density. However, the variable density introduces considerable difficulties for the construction and analysis of accurate and stable projection type schemes. For example, it is well known that the skew-symmetry of the nonlinear term in the Navier–Stokes equations (with constant density ρ_0), namely,

$$\int_{\Omega} (\rho_0 \mathbf{u} \cdot \nabla)\mathbf{v} \cdot \mathbf{v} \, d\mathbf{x} = 0 \quad \text{for } \mathbf{u}, \mathbf{v} \text{ smooth enough and } \mathbf{u} \cdot \mathbf{v}|_{\Gamma} = 0,$$

plays a very important role in the analysis of the Navier–Stokes equations and the corresponding numerical schemes. However, this property no longer holds when ρ is not a constant. To overcome this difficulty, Guermond and Quartapelle [6] considered the following system in conserved form:

$$\rho_t + \mathbf{u} \cdot \nabla\rho + \frac{\rho}{2}\nabla \cdot \mathbf{u} = 0, \tag{1.3a}$$

$$\sigma(\sigma\mathbf{u})_t + (\rho\mathbf{u} \cdot \nabla)\mathbf{u} + \frac{\mathbf{u}}{2}\nabla \cdot (\rho\mathbf{u}) + \nabla p - \mu\Delta\mathbf{u} = \mathbf{f} \quad \text{in } \Omega \times (0, T], \tag{1.3b}$$

$$\nabla \cdot \mathbf{u} = 0, \tag{1.3c}$$

where $\sigma = \sqrt{\rho}$. Note that the term $\frac{\rho}{2}\nabla \cdot \mathbf{u}$, which is zero everywhere due to (1.3c), is kept in the formulation in anticipation that the incompressibility condition (1.3c) may not be satisfied exactly in the space discrete case.

We derive from (1.1a) and (1.1c) that

$$\sigma(\sigma\mathbf{u})_t = \rho\mathbf{u}_t + \frac{1}{2}\rho_t\mathbf{u} = \rho\mathbf{u}_t - \frac{1}{2}\nabla \cdot (\rho\mathbf{u})\mathbf{u}.$$

Hence, the system (1.3) is mathematically equivalent to the original system (1.1), but now the nonlinear terms in (1.3) satisfy the desired properties that for ρ, $\mathbf{u}$, $\mathbf{v}$ smooth enough and $\mathbf{u} \cdot \mathbf{v}|_{\Gamma} = 0$, we have

$$\int_{\Omega} \mathbf{u} \cdot \nabla\rho \cdot \rho \, dx = 0 \quad \text{and} \quad \frac{1}{2}\int_{\Omega} \rho\nabla \cdot \mathbf{u}\rho \, dx = 0, \tag{1.4}$$

$$\int_{\Omega} (\rho\mathbf{u} \cdot \nabla)\mathbf{v} \cdot \mathbf{v} \, dx + \frac{1}{2}\int_{\Omega} \nabla \cdot (\rho\mathbf{u})\mathbf{v} \cdot \mathbf{v} \, dx = 0. \tag{1.5}$$

Hence, taking the inner product of (1.3a) with $\rho(\mathbf{x}, t)$ and of (1.3b) with $\mathbf{u}(\mathbf{x}, t)$, we obtain the following identities:

$$\frac{1}{2}\frac{d}{dt}\|\rho(\cdot, t)\|_{L^2}^2 = 0,$$

$$\frac{1}{2}\frac{d}{dt}\|\sigma(t)\mathbf{u}(\cdot, t)\|_{L^2}^2 + \mu\|\nabla\mathbf{u}(\cdot, t)\|_{L^2}^2 = \int_{\Omega} \mathbf{f}(\mathbf{x}, t) \cdot \mathbf{u}(\mathbf{x}, t) \, d\mathbf{x}.$$

It is from this conserved formulation that Guermond and Quartapelle were able to construct some stable projection type schemes for the incompressible flows with variable density and proved rigorously their stability in [6]. To the best of our knowledge, the stability analysis [6] is still the only rigorous proof available for any projection type scheme with variable density. However, for the more accurate version (see (4.1)–(4.5) in [6]) which is based on the incremental projection scheme (i.e., the pressure-correction scheme), two projection steps (i.e., two pressure-Poisson solvers) are needed to preserve the stability of the scheme. Since the pressure-Poisson solver consumes a significant part (it is often the most time consuming part) of the total computational effort, this approach could increase the total computational cost significantly as opposed to the schemes with only one projection step. On the other hand, while the system in conserved form (1.3) is convenient for analysis, it does involve additional cost in computing the two additional nonlinear terms in (1.3a) and (1.3b). In some cases where a non-variational method such as spectral-collocation method or finite difference method is used, it is often not advisable to use (1.3). Hence, it is also of interest to have a stable numerical scheme which is based on the original system (1.1).

The purpose of this paper is to propose two new Gauge–Uzawa schemes for incompressible flows with variable density. The first scheme will be based on the system in conserved form (1.3) while the second scheme will be based on the system in convected form (1.1). We recall that the Gauge–Uzawa method is introduced in [12,10] to overcome some implementation difficulties associated with the Gauge method introduced in [3]. It has been shown in [12,10,13,11] that the Gauge–Uzawa method has many advantages over the original Gauge method and the pressure-correction method. We will show that a proper Gauge–Uzawa formulation is well suitable for problems with variable density. More precisely, our two new schemes will only involve one projection step and will be proved unconditionally stable.

The paper is organized as follows. In the next two sections, we present the two Gauge–Uzawa schemes and show that they are unconditionally stable, respectively. In Section 4, we present some numerical results which reveal the convergence rate of our schemes for each of the three unknown functions. We also present a challenging numerical simulation of an air bubble rising in water. some concluding remarks are given in Section 5.

We now introduce some notations. We denote by $H^s(\Omega)$ and $H_0^s(\Omega)$ the usual Sobolev spaces. Let $d = 2$ or 3 be the space dimension. We set $\mathbf{L}^2(\Omega) := (L^2(\Omega))^d$ and $\mathbf{H}^s(\Omega) := (H^s(\Omega))^d$, and denote by $L_0^2(\Omega)$ the subspace of $L^2(\Omega)$ of functions with vanishing mean-value. We use $\|\cdot\|_s$ to denote the norm in $H^s(\Omega)$ and $\langle\cdot,\cdot\rangle$ to denote the inner product in $L^2(\Omega)$.

2. Gauge–Uzawa method in conserved form

2.1. The scheme and its stability

The first-order semi-discrete Gauge–Uzawa method based on the conserved system (1.3) reads as follows:

Algorithm 1 (*Gauge–Uzawa method in conserved form*). Set $\rho^0 = \rho_0$, $\mathbf{u}^0 = \mathbf{u}_0$ and $s^0 = 0$; repeat for $1 \leqslant n \leqslant N \leqslant T/\tau - 1$:

Step 1. Find ρ^{n+1} as the solution of

$$\begin{cases} \frac{\rho^{n+1}-\rho^n}{\tau} + \mathbf{u}^n \cdot \nabla\rho^{n+1} + \frac{\rho^{n+1}}{2}\nabla\cdot\mathbf{u}^n = 0, \\ \rho^{n+1}|_{\Gamma_{\mathbf{u}^n}} = r^{n+1}. \end{cases} \tag{2.1}$$

Step 2. Find $\widehat{\mathbf{u}}^{n+1}$ as the solution of

$$\begin{cases} \sigma^{n+1}\frac{\sigma^{n+1}\widehat{\mathbf{u}}^{n+1}-\sigma^n\mathbf{u}^n}{\tau} + \rho^{n+1}(\mathbf{u}^n\cdot\nabla)\widehat{\mathbf{u}}^{n+1} + \frac{1}{2}(\nabla\cdot(\rho^{n+1}\mathbf{u}^n))\widehat{\mathbf{u}}^{n+1} + \mu\nabla s^n - \mu\Delta\widehat{\mathbf{u}}^{n+1} = \mathbf{f}^{n+1}, \\ \widehat{\mathbf{u}}^{n+1}|_\Gamma = \mathbf{g}^{n+1}. \end{cases} \tag{2.2}$$

Step 3. Find ϕ^{n+1} as the solution of

$$\begin{cases} -\nabla\cdot\left(\frac{1}{\rho^{n+1}}\nabla\phi^{n+1}\right) = \nabla\cdot\widehat{\mathbf{u}}^{n+1}, \\ \partial_\nu\phi^{n+1}|_\Gamma = 0. \end{cases} \tag{2.3}$$

Step 4. Update $\mathbf{u}^{n+1}$ and s^{n+1} by

$$\mathbf{u}^{n+1} = \widehat{\mathbf{u}}^{n+1} + \frac{1}{\rho^{n+1}}\nabla\phi^{n+1},$$
$$s^{n+1} = s^n - \nabla\cdot\widehat{\mathbf{u}}^{n+1}. \tag{2.4}$$

Remark 2.1. In practice, (2.3) is often reformulated in the following weak formulation

$$\left\langle \frac{1}{\rho^{n+1}}\nabla\phi^{n+1}, \nabla q \right\rangle = -\langle\widehat{\mathbf{u}}^{n+1}, \nabla q\rangle \quad \forall q \in H^1(\Omega), \tag{2.5}$$

and then discretized. We derive immediately from (2.5, 2.4) that

$$\langle\mathbf{u}^{n+1}, \nabla q\rangle = 0 \quad \forall q \in H^1(\Omega), \tag{2.6}$$

which implies that in the space continuous case, we have

$$\nabla\cdot\mathbf{u}^{n+1} = 0 \quad \text{and} \quad \mathbf{u}^{n+1}\cdot\mathbf{v}|_\Gamma = \mathbf{g}^{n+1}\cdot\mathbf{v}|_\Gamma. \tag{2.7}$$

However, in the space discrete case, only a discrete version of (2.6) will be satisfied so the discrete velocity field will generally not be divergence free.

Remark 2.2. Note that the pressure does not appear in the above algorithm. However, a proper approximation of the pressure can be constructed. To this end, let us assume for the moment $\rho = \rho_0$ is a constant and drop the nonlinear terms. Then, eliminating $\widehat{\mathbf{u}}^{n+1}$ from (2.2) using (2.4) and (2.7) leads to

$$\rho_0\frac{\mathbf{u}^{n+1} - \mathbf{u}^n}{\tau} - \mu\Delta\mathbf{u}^{n+1} + \nabla(\mu s^{n+1} - \frac{1}{\tau}\phi^{n+1}) = \mathbf{f}^{n+1},$$
$$\nabla\cdot\mathbf{u}^{n+1} = 0, \mathbf{u}^{n+1}\cdot\mathbf{v}|_\Gamma = \mathbf{g}^{n+1}\cdot\mathbf{v}|_\Gamma.$$

Hence, we should define the pressure approximation as

$$p^{n+1} = -\frac{1}{\tau}\phi^{n+1} + \mu s^{n+1}. \tag{2.8}$$

Next, we establish a stability result. For the sake of simplicity, we shall consider only homogeneous Dirichlet boundary conditions for the velocity, i.e., $\mathbf{u}|_\Gamma = 0$.

Theorem 2.1. *Assuming* $\mathbf{g} \equiv 0$, *the Gauge–Uzawa Algorithm* 1 *is unconditionally stable in the sense that, for all* $\tau > 0$ *and* $0 \leqslant N \leqslant T/\tau - 1$, *the following a priori bounds hold*:

$$\|\rho^{N+1}\|_0^2 + \sum_{n=0}^{N}\|\rho^{n+1} - \rho^n\|_0^2 = \|\rho^0\|_0^2 \tag{2.9}$$

and

$$\|\sigma^{N+1}\widehat{\mathbf{u}}^{N+1}\|_0^2 + \sum_{n=1}^{N}\left(\|\sigma^{n+1}\widehat{\mathbf{u}}^{n+1} - \sigma^n\mathbf{u}^n\|_0^2 + \|\frac{1}{\sigma^n}\nabla\phi^n\|_0^2\right) + \mu\tau\|s^{N+1}\|_0^2 + \frac{\mu}{2}\tau\sum_{n=1}^{N}\|\nabla\widehat{\mathbf{u}}^{n+1}\|_0^2$$
$$\leqslant \|\sigma^0\widehat{\mathbf{u}}^0\|_0^2 + C\mu\tau\sum_{n=1}^{N}\|\mathbf{f}^{n+1}\|_{-1}^2. \tag{2.10}$$

Proof. Taking the inner product of (2.1) with $2\tau\rho^{n+1}$, thanks to (1.4), we get

$$\|\rho^{n+1}\|_0^2 + \|\rho^{n+1} - \rho^n\|_0^2 - \|\rho^n\|_0^2 = 0.$$

Summing it over *n* from 0 to *N* leads to (2.9).

Next, we take the inner product of (2.2) with $2\tau\widehat{\mathbf{u}}^{n+1}$, thanks to (1.5), we get

$$\|\sigma^{n+1}\widehat{\mathbf{u}}^{n+1}\|_0^2 + \|\sigma^{n+1}\widehat{\mathbf{u}}^{n+1} - \sigma^n\mathbf{u}^n\|_0^2 - \|\sigma^n\mathbf{u}^n\|_0^2 + 2\mu\tau\|\nabla\widehat{\mathbf{u}}^{n+1}\|_0^2 + 2\mu\tau\langle\nabla s^n, \widehat{\mathbf{u}}^{n+1}\rangle = 2\mu\tau\langle\mathbf{f}^{n+1}, \widehat{\mathbf{u}}^{n+1}\rangle. \quad (2.11)$$

The next task is to derive a suitable relation between $\|\sigma^n\mathbf{u}^n\|_0^2$ and $\|\sigma^n\widehat{\mathbf{u}}^n\|_0^2$ so that we can sum over n the relation (2.11). To this end, we derive from (2.3) and (2.6) that

$$\|\sigma^n\mathbf{u}^n\|_0^2 = \langle\rho^n\mathbf{u}^n, \mathbf{u}^n\rangle = \langle\rho^n\widehat{\mathbf{u}}^n + \nabla\phi^n, \mathbf{u}^n\rangle = \langle\rho^n\widehat{\mathbf{u}}^n, \mathbf{u}^n\rangle = \left\langle\rho^n\widehat{\mathbf{u}}^n, \widehat{\mathbf{u}}^n + \frac{1}{\rho^n}\nabla\phi^n\right\rangle$$

$$= \|\sigma^n\widehat{\mathbf{u}}^n\|_0^2 + \left\langle\mathbf{u}^n - \frac{1}{\rho^n}\nabla\phi^n, \nabla\phi^n\right\rangle = \|\sigma^n\widehat{\mathbf{u}}^n\|_0^2 - \|\frac{1}{\sigma^n}\nabla\phi^n\|_0^2. \quad (2.12)$$

We now sum up (2.11) and (2.12) to get

$$\|\sigma^{n+1}\widehat{\mathbf{u}}^{n+1}\|_0^2 - \|\sigma^n\widehat{\mathbf{u}}^n\|_0^2 + \|\frac{1}{\sigma^n}\nabla\phi^n\|_0^2 + \|\sigma^{n+1}\widehat{\mathbf{u}}^{n+1} - \sigma^n\mathbf{u}^n\|_0^2 + 2\mu\tau\|\nabla\widehat{\mathbf{u}}^{n+1}\|_0^2 = A_1 + A_2 \quad (2.13)$$

with

$$\begin{aligned} A_1 &:= 2\mu\tau\langle s^n, \nabla\cdot\widehat{\mathbf{u}}^{n+1}\rangle, \\ A_2 &:= 2\mu\tau\langle\mathbf{f}^{n+1}, \widehat{\mathbf{u}}^{n+1}\rangle. \end{aligned} \quad (2.14)$$

We derive from the well-known inequality

$$\|\nabla\cdot\mathbf{v}\|_0 \leqslant \|\nabla\mathbf{v}\|_0 \quad \forall\mathbf{v}\in\mathbf{H}_0^1(\Omega), \quad (2.15)$$

and (2.4) that

$$A_1 = -2\mu\tau\langle s^n, s^{n+1} - s^n\rangle = -\mu\tau(\|s^{n+1}\|_0^2 - \|s^{n+1} - s^n\|_0^2 - \|s^n\|_0^2)$$

$$= -\mu\tau(\|s^{n+1}\|_0^2 - \|s^n\|_0^2) + \mu\tau\|\nabla\cdot\widehat{\mathbf{u}}^{n+1}\|_0^2 \leqslant -\mu\tau(\|s^{n+1}\|_0^2 - \|s^n\|_0^2) + \mu\tau\|\nabla\widehat{\mathbf{u}}^{n+1}\|_0^2. \quad (2.16)$$

Using the Cauchy-Schwarz inequality, we find

$$A_2 \leqslant C\mu\tau\|\mathbf{f}^{n+1}\|_{-1}^2 + \frac{\mu}{2}\tau\|\nabla\widehat{\mathbf{u}}^{n+1}\|_0^2. \quad (2.17)$$

Inserting the above two results into (2.13) leads to

$$\|\sigma^{n+1}\widehat{\mathbf{u}}^{n+1}\|_0^2 - \|\sigma^n\widehat{\mathbf{u}}^n\|_0^2 + \mu\tau\|s^{n+1}\|_0^2 - \mu\tau\|s^n\|_0^2 + \|\frac{1}{\sigma^n}\nabla\phi^n\|_0^2 + \|\sigma^{n+1}\widehat{\mathbf{u}}^{n+1} - \sigma^n\mathbf{u}^n\|_0^2 + \frac{\mu}{2}\tau\|\nabla\widehat{\mathbf{u}}^{n+1}\|_0^2$$

$$\leqslant C\mu\tau\|\mathbf{f}^{n+1}\|_{-1}^2.$$

Summing the above over n from 0 to N yields (2.10). $\quad\square$

2.2. A finite element discretization

We now describe, as an example of space discretizations, a finite element method for Algorithm 1. Let $\Sigma = \{K\}$ be a shape regular quasi-uniform partition of Ω with mesh-size h. We define

$$\begin{aligned} \mathbb{W}_h &= \{\phi_h \in L^2(\Omega) : \phi_h|_K \in \mathscr{P}(K) \quad \forall K \in \Sigma\}, \\ \mathbb{Q}_h &= \{q_h \in L_0^2(\Omega) \cap C(\Omega) : q_h|_K \in \mathscr{Q}(K) \quad \forall K \in \Sigma\}, \\ \mathbb{V}_h^b &= \{\mathbf{v}_h \in \mathbf{C}(\Omega) : \mathbf{v}_h|_K \in \mathscr{R}(K) \quad \forall K \in \Sigma; \mathbf{v}_h|_\Gamma = b\}, \end{aligned}$$

where, for all $K \in \Sigma$, $\mathscr{P}(K)$, $\mathscr{Q}(K)$ and $\mathscr{R}(K)$ are spaces of polynomials with degree $\mathscr{P}$, $\mathscr{Q}$ and $\mathscr{R}$, respectively. Then, the FEM Gauge–Uzawa method reads as follows:

FEM Gauge–Uzawa method. Let ρ_{0h} and $\mathbf{u}_{0h}$ be a suitable approximation of ρ_0 and $\mathbf{u}_0$, respectively. Set $\rho_h^0 = \rho_{0h}, \mathbf{u}_h^0 = \mathbf{u}_{0h}$ and $s_h^0 = 0$; repeat for $1 \leqslant n \leqslant N \leqslant T/\tau - 1$:

Step 1. Find $\rho_h^{n+1} \in \mathbb{W}_h$ such that

$$\begin{cases} \left\langle \frac{\rho_h^{n+1} - \rho_h^n}{\tau} + \mathbf{u}_h^n \cdot \nabla \rho_h^{n+1} + \frac{\rho_h^{n+1}}{2} \nabla \cdot \mathbf{u}_h^n, \psi_h \right\rangle = 0 \quad \forall \psi_h \in \mathbb{W}_h, \\ \rho_h^{n+1}|_{\Gamma_{\mathbf{u}^n}} = r_h^{n+1}. \end{cases} \tag{2.18}$$

Step 2. Find $\widehat{\mathbf{u}}_h^{n+1} \in \mathbb{V}_h^{\mathbf{g}^{n+1}}$ such that

$$\left\langle \sigma_h^{n+1} \frac{\sigma_h^{n+1} \widehat{\mathbf{u}}_h^{n+1} - \sigma_h^n \mathbf{u}_h^n}{\tau}, \mathbf{w}_h \right\rangle + \langle \rho_h^{n+1} (\mathbf{u}_h^n \cdot \nabla) \widehat{\mathbf{u}}_h^{n+1}, \mathbf{w}_h \rangle + \frac{1}{2} \langle (\nabla \cdot (\rho_h^{n+1} \mathbf{u}_h^n)) \widehat{\mathbf{u}}_h^{n+1}, \mathbf{w}_h \rangle - \mu \langle s_h^n, \nabla \cdot w_h \rangle$$
$$+ \mu \langle \nabla \widehat{\mathbf{u}}_h^{n+1}, \nabla \widehat{\mathbf{u}}_h^{n+1} \rangle = \langle \mathbf{f}_h(t^{n+1}), w_h \rangle \quad \forall V_h \in \mathbb{V}_h^0. \tag{2.19}$$

Step 3. Find $\phi_h^{n+1} \in \mathbb{Q}_h$ such that

$$\left\langle \frac{1}{\rho_h^{n+1}} \nabla \phi_h^{n+1}, \nabla q_h \right\rangle = -\langle \widehat{\mathbf{u}}_h^{n+1}, \nabla q_h \rangle \quad \forall q_h \in \mathbb{Q}_h. \tag{2.20}$$

Step 4. Update $\mathbf{u}_h^{n+1}$ and $s_h^{n+1} \in \mathbb{Q}_h$ by

$$\mathbf{u}_h^{n+1} = \widehat{\mathbf{u}}_h^{n+1} + \frac{1}{\rho_h^{n+1}} \nabla \phi_h^{n+1},$$
$$\langle s_h^{n+1}, q_h \rangle = \langle s_h^n - \nabla \cdot \widehat{\mathbf{u}}_h^{n+1}, q_h \rangle \quad \forall q_h \in \mathbb{Q}_h. \tag{2.21}$$

Remark 2.3. We recall that in proving Theorem 2.1, we did not use *directly* the incompressibility condition. In fact, only the properties (1.4), (1.5) and (2.6) were used. Since we derive from (2.20) and (2.21) that

$$\langle \mathbf{u}_h^{n+1}, \nabla q_h \rangle = 0 \quad \forall q_h \in \mathbb{Q}_h$$

so the proof of Theorem 2.1 can be carried over to this discrete case and the stability results in Theorem 2.1 are also valid with all quantities replaced by their discrete counterparts.

Note that $\mathbf{u}_h^n$ computed from (2.21) lives in a strange space which is not convenient for implementation and for analysis. However, it is clear that one may completely eliminate $\mathbf{u}_h^n$ from the above algorithm to avoid this difficulty.

The solution of the discrete density Eq. (2.18) presents the usual difficulties associated with Galerkin FEM for hyperbolic equations (see, for instance, [7,4]). Many finite element techniques have been developed to overcome these difficulties, e.g., streamline diffusion [7], discontinuous Galerkin [7], artificial diffusion [7], sub-grid discretization or least-squares [4], and so on. In the numerical results presented below, we adopted a least-square method which we briefly describe now. To simplify the presentation, we consider the simple equation

$$\rho + \alpha \mathbf{U} \cdot \nabla \rho = f, \tag{2.22}$$

where α is a given constant and $\mathbf{U}$ is a given velocity with $\nabla \cdot \mathbf{U} = 0$ and $\mathbf{U} \cdot \mathbf{v}|_\Gamma = 0$. The *Least-Squares* method can be derived by taking the inner product of (2.22) with $\psi + \alpha \mathbf{U} \cdot \nabla \psi$:

$$\langle \rho + \alpha \mathbf{U} \cdot \nabla \rho, \psi + \alpha \mathbf{U} \cdot \nabla \psi \rangle = \langle f, \psi + \alpha \mathbf{U} \cdot \nabla \psi \rangle. \tag{2.23}$$

Since $\nabla \cdot \mathbf{U} = 0$ and $\mathbf{U} \cdot \mathbf{v} = 0$, we have $\langle \mathbf{U} \cdot \nabla \rho, \psi \rangle = -\langle \mathbf{U} \cdot \nabla \psi, \rho \rangle$. So (2.23) can be rewritten as

$$\langle \rho, \psi \rangle + \alpha^2 \langle \mathbf{U} \cdot \nabla \rho, \mathbf{U} \cdot \nabla \psi \rangle = \langle f, \psi + \alpha \mathbf{U} \cdot \nabla \psi \rangle.$$

We then define the *Least-squares* method as: find $\rho_h \in \mathbb{V}_h$ such that

$$\langle \rho_h, \psi_h \rangle + \alpha^2 \langle \mathbf{U} \cdot \nabla \rho_h, \mathbf{U} \cdot \nabla \psi_h \rangle = \langle f, \psi_h + \alpha \mathbf{U} \cdot \nabla \psi_h \rangle \quad \forall \psi_h \in \mathbb{V}_h.$$

We indicate that, unlike the standard Galerkin formulation, the above linear system is *symmetric* and we have the following error bound (cf. [4]):

$$\|\rho - \rho_h\|_0 + \|\mathbf{U} \cdot \nabla(\rho - \rho_h)\|_0 \leqslant Ch^\gamma \|\rho\|_{\gamma+1}.$$

Note that this estimate is optimal in the norm induced by the stream-wise derivative but is only sub-optimal in the L^2-norm as is in the standard Galerkin method.

2.3. A second-order version

Algorithm 1 is only first-order accurate. However, a second-order version with essentially the same computational procedures can be constructed as follows. For simplicity, we denote, for any function a, its second-order extrapolation by $\overline{a}^{n+1} = 2a^n - a^{n-1}$.

A second-order Gauge–Uzawa method. Set $\rho^0 = \rho_0$, $\mathbf{u}^0 = \mathbf{u}_0$ and $s^0 = 0$ and compute $\mathbf{u}^1$, ϕ^1, s^1, p^1 with Algorithm 1; repeat for $2 \leqslant n \leqslant N \leqslant T/\tau - 1$.

Step 1. Find ρ^{n+1} as the solution of

$$\begin{cases} \frac{3\rho^{n+1}-4\rho^n+\rho^{n-1}}{2\tau} + \overline{\mathbf{u}}^{n+1} \cdot \nabla\rho^{n+1} + \frac{\rho^{n+1}}{2}\nabla \cdot \overline{\mathbf{u}}^{n+1} = 0, \\ \rho^{n+1}|_{\Gamma_{\overline{\mathbf{u}}^{n+1}}} = r^{n+1}. \end{cases} \tag{2.24}$$

Step 2. Find $\widehat{\mathbf{u}}^{n+1}$ as the solution of

$$\begin{cases} \rho^{n+1}\frac{3\widehat{\mathbf{u}}^{n+1}-4\mathbf{u}^n+\mathbf{u}^{n-1}}{2\tau} + \rho^{n+1}(\overline{\mathbf{u}}^{n+1} \cdot \nabla)\widehat{\mathbf{u}}^{n+1} + \frac{1}{2}(\nabla \cdot (\rho^{n+1}\overline{\mathbf{u}}^{n+1}))\widehat{\mathbf{u}}^{n+1} + \nabla p^n + \mu\nabla s^n - \mu\Delta\widehat{\mathbf{u}}^{n+1} = \mathbf{f}^{n+1}, \\ \widehat{\mathbf{u}}^{n+1}|_\Gamma = \mathbf{g}^{n+1}. \end{cases} \tag{2.25}$$

Step 3. Find ϕ^{n+1} as the solution of

$$\left\{ -\nabla \cdot \left(\frac{1}{\rho^{n+1}}\nabla\phi^{n+1}\right) = \nabla \cdot \widehat{\mathbf{u}}^{n+1}, \partial_\nu\phi^{n+1}|_\Gamma = 0. \right. \tag{2.26}$$

Step 4. Update $\mathbf{u}^{n+1}$, s^{n+1} and p^{n+1} by

$$\begin{aligned} \mathbf{u}^{n+1} &= \widehat{\mathbf{u}}^{n+1} + \frac{1}{\rho^{n+1}}\nabla\phi^{n+1}, \\ s^{n+1} &= s^n - \nabla \cdot \widehat{\mathbf{u}}^{n+1}, \\ p^{n+1} &= p^n - \frac{3\phi^{n+1}}{2\tau} + \mu s^{n+1}. \end{aligned} \tag{2.27}$$

To see that the above scheme is indeed (formally) second-order accurate, we drop the nonlinear terms and consider $\rho = \rho_0$ (note that it is obvious that the approximations for the nonlinear terms and the density are second-order), after eliminating $\widehat{\mathbf{u}}^{n+1}$, we find

$$\begin{aligned} \rho_0 \frac{3\mathbf{u}^{n+1} - 4\mathbf{u}^n + \mathbf{u}^{n-1}}{2\tau} - \mu\Delta\mathbf{u}^{n+1} + \nabla p^{n+1} &= \mathbf{f}^{n+1}, \\ \nabla \cdot \mathbf{u}^{n+1} = 0, \mathbf{u}^{n+1} \cdot \boldsymbol{\nu}|_\Gamma &= 0. \end{aligned}$$

Hence, the scheme is formally second-order accurate.

However, although ample numerical experiments indicate that this scheme is unconditionally stable, how to prove the unconditional stability is an open problem. In fact, how to prove the stability of the above algorithm without the nonlinear terms and with constant density is still an open problem.

3. Gauge–Uzawa method in convective form

As we mentioned in the introduction, in some cases where a non-variational method such as spectral-collocation method or finite difference method is used, it is often desirable to use numerical algorithms based on the original system in convective form.

Algorithm 2 (*Gauge–Uzawa method in convective form*). Set $\rho^0 = \rho_0$, $\mathbf{u}^0 = \mathbf{u}_0$ and $s^0 = 0$; repeat for $1 \leqslant n \leqslant N \leqslant T/\tau - 1$:

Step 1. Find ρ^{n+1} as the solution of

$$
\begin{cases}
\frac{\rho^{n+1}-\rho^n}{\tau} + \mathbf{u}^n \cdot \nabla \rho^{n+1} = 0, \\
\rho^{n+1}|_{\Gamma_{\mathbf{u}^n}} = r^{n+1}.
\end{cases}
\tag{3.1}
$$

Step 2. Find $\widehat{\mathbf{u}}^{n+1}$ as the solution of

$$
\begin{cases}
\rho^n \frac{\widehat{\mathbf{u}}^{n+1}-\mathbf{u}^n}{\tau} + \rho^{n+1}(\mathbf{u}^n \cdot \nabla)\widehat{\mathbf{u}}^{n+1} + \mu\nabla s^n - \mu\Delta\widehat{\mathbf{u}}^{n+1} = \mathbf{f}^{n+1}, \\
\widehat{\mathbf{u}}^{n+1}|_\Gamma = \mathbf{g}^{n+1}.
\end{cases}
\tag{3.2}
$$

Step 3. Find ϕ^{n+1} as the solution of

$$
\begin{cases}
-\nabla \cdot \left(\frac{1}{\rho^{n+1}}\nabla\phi^{n+1}\right) = \nabla \cdot \widehat{\mathbf{u}}^{n+1}, \\
\partial_\nu\phi^{n+1}|_\Gamma = 0.
\end{cases}
$$

Step 4. Update $\mathbf{u}^{n+1}$ and s^{n+1} by

$$
\mathbf{u}^{n+1} = \widehat{\mathbf{u}}^{n+1} + \frac{1}{\rho^{n+1}}\nabla\phi^{n+1},
$$

$$
s^{n+1} = s^n - \nabla \cdot \widehat{\mathbf{u}}^{n+1}.
$$

Remark 3.1. Once again, the pressure does not appear directly in the algorithm but an approximation of the pressure can be defined by (2.8).

A second-order version of this algorithm can be similarly constructed as in Eqs. (2.24)–(2.27).

We now present a stability result. As in Theorem 2.1, we shall consider, for the sake of simplicity, only homogeneous Dirichlet boundary conditions for the velocity, i.e., $\mathbf{u}|_\Gamma = 0$.

Theorem 3.1. *Assuming* $\mathbf{g} \equiv 0$, *the Gauge–Uzawa Algorithm 2 is unconditionally stable in the sense that, for all* $\tau > 0$ *and* $0 \leqslant N \leqslant T/\tau - 1$, *the following a priori bounds hold*:

$$
\|\rho^{N+1}\|_0^2 + \sum_{n=0}^{N} \|\rho^{n+1} - \rho^n\|_0^2 = \|\rho^0\|_0^2
\tag{3.3}
$$

and

$$
\|\sigma^{N+1}\widehat{\mathbf{u}}^{n+1}\|_0^2 + \sum_{n=0}^{N}\left(\|\sigma^n(\widehat{\mathbf{u}}^{n+1}-\mathbf{u}^n)\|_0^2 + \left\|\frac{1}{\sigma^n}\nabla\phi^n\right\|_0^2\right) + \mu\tau\|s^{N+1}\|_0^2 + \frac{\mu}{2}\tau\sum_{n=0}^{N}\|\nabla\widehat{\mathbf{u}}^{n+1}\|_0^2
$$

$$
\leqslant \|\sigma^0\widehat{\mathbf{u}}^0\|_0^2 + C\mu\tau\sum_{n=0}^{N}\|\mathbf{f}^{n+1}\|_{-1}^2.
\tag{3.4}
$$

Proof. Taking the inner product of (3.1) with $2\tau\rho^{n+1}$, thanks to the first equation in (1.4), we have

$$
\|\rho^{n+1}\|_0^2 + \|\rho^{n+1} - \rho^n\|_0^2 - \|\rho^n\|_0^2 = 0.
$$

Summing up over n from 0 to N leads to (3.3).

Next, taking the inner product of (3.2) with $2\tau\widehat{\mathbf{u}}^{n+1}$, we find

$$
2\langle\rho^n(\widehat{\mathbf{u}}^{n+1}-\mathbf{u}^n), \widehat{\mathbf{u}}^{n+1}\rangle + 2\tau\langle\rho^{n+1}(\mathbf{u}^n \cdot \nabla)\widehat{\mathbf{u}}^{n+1}, \widehat{\mathbf{u}}^{n+1}\rangle + 2\mu\tau\langle\nabla s^n, \widehat{\mathbf{u}}^{n+1}\rangle + 2\mu\tau\|\nabla\widehat{\mathbf{u}}^{n+1}\|_0^2
$$
$$
= 2\mu\tau\langle\mathbf{f}^{n+1}, \widehat{\mathbf{u}}^{n+1}\rangle.
\tag{3.5}
$$

Setting $\sigma^n = \sqrt{\rho^n}$, we can write the first term in the above as

$$
2\langle\rho^n(\widehat{\mathbf{u}}^{n+1}-\mathbf{u}^n), \widehat{\mathbf{u}}^{n+1}\rangle = \|\sigma^n\widehat{\mathbf{u}}^{n+1}\|_0^2 + \|\sigma^n(\widehat{\mathbf{u}}^{n+1}-\mathbf{u}^n)\|_0^2 - \|\sigma^n\mathbf{u}^n\|_0^2.
\tag{3.6}
$$

The relation (2.12) is still valid so we only need to derive a suitable relation between $\|\sigma^n\widehat{\mathbf{u}}^{n+1}\|_0^2$ and $\|\sigma^{n+1}\widehat{\mathbf{u}}^{n+1}\|_0^2$. To this end, we take the inner product of (3.1) with a scalar function $\tau\widehat{\mathbf{u}}^{n+1} \cdot \widehat{\mathbf{u}}^{n+1}$ to get

$$\langle \rho^{n+1} - \rho^n, \widehat{\mathbf{u}}^{n+1} \cdot \widehat{\mathbf{u}}^{n+1} \rangle = -\tau \langle \nabla \cdot (\rho^{n+1} \mathbf{u}^n), \widehat{\mathbf{u}}^{n+1} \cdot \widehat{\mathbf{u}}^{n+1} \rangle, \tag{3.7}$$

which can be rewritten as

$$\|\sigma^{n+1} \widehat{\mathbf{u}}^{n+1}\|_0^2 - \|\sigma^n \widehat{\mathbf{u}}^{n+1}\|_0^2 = 2\tau \langle \rho^{n+1} (\mathbf{u}^n \cdot \nabla) \widehat{\mathbf{u}}^{n+1}, \widehat{\mathbf{u}}^{n+1} \rangle. \tag{3.8}$$

Combining (3.8) and (2.12) into (3.6), we obtain

$$2\langle \rho^n (\widehat{\mathbf{u}}^{n+1} - \mathbf{u}^n), \widehat{\mathbf{u}}^{n+1} \rangle + 2\tau \langle \rho^{n+1} (\mathbf{u}^n \cdot \nabla) \widehat{\mathbf{u}}^{n+1}, \widehat{\mathbf{u}}^{n+1} \rangle$$

$$= \|\sigma^{n+1} \widehat{\mathbf{u}}^{n+1}\|_0^2 + \|\sigma^n (\widehat{\mathbf{u}}^{n+1} - \mathbf{u}^n)\|_0^2 - \|\sigma^n \widehat{\mathbf{u}}^n\|_0^2 + \left\| \frac{1}{\sigma^n} \nabla \phi^n \right\|_0^2.$$

Now, replacing the first two terms in (3.5) by the above leads to

$$\|\sigma^{n+1} \widehat{\mathbf{u}}^{n+1}\|_0^2 + \|\sigma^n (\widehat{\mathbf{u}}^{n+1} - \mathbf{u}^n)\|_0^2 - \|\sigma^n \widehat{\mathbf{u}}^n\|_0^2 + \left\| \frac{1}{\sigma^n} \nabla \phi^n \right\|_0^2 + 2\mu\tau \|\nabla \widehat{\mathbf{u}}^{n+1}\|_0^2 = A_1 + A_2$$

with A_1 and A_2 defined in (2.14). Using the estimates (2.16) and (2.17) yields

$$\|\sigma^{n+1} \widehat{\mathbf{u}}^{n+1}\|_0^2 + \|\sigma^n (\widehat{\mathbf{u}}^{n+1} - \widehat{\mathbf{u}}^n)\|_0^2 - \|\sigma^n \widehat{\mathbf{u}}^n\|_0^2 + \frac{\mu}{2}\tau \|\nabla \widehat{\mathbf{u}}^{n+1}\|_0^2 + \left\| \frac{1}{\sigma^n} \nabla \phi^n \right\|_0^2 + \mu\tau(\|s^{n+1}\|_0^2 - \|s^n\|_0^2)$$

$$\leqslant C\mu\tau \|\mathbf{f}^{n+1}\|_{-1}^2.$$

Summing up the above over n from 0 to N leads to (3.4). $\square$

Remark 3.2. How to design a suitable space discretization for Algorithm 2 and prove its stability is a more complicate issue.

First of all, (3.7) indicates that the polynomial degree for the density ρ may have to be twice that of the velocity $\mathbf{u}$. Secondly, the incompressibility condition for $\mathbf{u}^n$ plays an essential role in the stability proof. Hence, in order to carry over the proof to the discrete case, one may need to reformulate Steps 3 and 4 in a mixed formulation to ensure that the finite dimensional approximation of $\mathbf{u}^{n+1}$ satisfies

$$\langle \nabla \cdot \mathbf{u}_h^{n+1}, q_h \rangle = 0 \quad \forall q_h \in \mathbb{Q}_h.$$

4. Numerical experiments

In this section, we present some computational experiments using the Gauge–Uzawa methods. Since the numerical results with the Gauge–Uzawa method in conserved form behave similarly with those with Gauge–Uzawa method in convective form, only the results with Gauge–Uzawa method in convective form will be presented.

In all the experiments, we use Taylor-Hood finite element for $(\mathbf{u}, p)$ and linear element for ρ, i.e., $(\mathscr{P}^1, \mathscr{P}^2, \mathscr{P}^1)$ for $(\rho, \mathbf{u}, p)$. Before performing the numerical experiments presented below, we have carried out a series of runs which confirmed that both the first- and second-order Gauge–Uzawa schemes in conserved form and in convective form are unconditionally stable.

4.1. Example 1: Accuracy check using an exact solution

In order to check the convergence rate of our numerical algorithms, we consider the exact solution used in [6]. The computational domain is the unit circle $|r| \leqslant 1$ and we choose an exact solution of (1.1) to be:

$$\begin{cases} \rho(x, y, t) = 2 + r\cos(\theta - \sin(t)), \\ u(x, y, t) = -y\cos(t), \\ v(x, y, t) = x\cos(t), \\ p(x, y, t) = \sin(x)\sin(y)\sin(t). \end{cases}$$

We set $\mu = 1$ and find the force function $\mathbf{f}$ to be:

$$\mathbf{f}(x,y,t) = \begin{pmatrix} (y\sin(t) - x\cos^2(t))\rho(x,y,t) + \cos(x)\sin(y)\sin(t) \\ -(x\sin(t) + y\cos^2(t))\rho(x,y,t) + \sin(x)\cos(y)\sin(t) \end{pmatrix}.$$

We choose the same mesh size for time and space $\tau = h$.

Let us denote

$$\varepsilon^{n+1} = \rho(t^{n+1}) - \rho^{n+1}, \quad \mathbf{E}^{n+1} = \mathbf{u}(t^{n+1}) - \mathbf{u}^{n+1}, \quad e^{n+1} = p(t^{n+1}) - p^{n+1}.$$

In Tables 1 and 2, the errors and convergence rates for the first-order and second-order Gauge–Uzawa methods in convective form are displayed respectively. We note that optimal convergence rates (in time) for all variables are observed for both the first- and second-order schemes.

Table 1
Error and convergence rate of the first-order Gauge–Uzawa scheme in convective form with finite element $(\mathscr{P}^1, \mathscr{P}^2, \mathscr{P}^1)$ for $(\rho, \mathbf{u}, p)$, $\mu = 1$ and $\tau = h$

$\tau = h$	1/8	1/16	1/32	1/64	1/128
$\|\varepsilon\|_{L^2}$	0.0439168	0.0226351	0.0114484	0.00574574	0.00287605
Order		0.956211	0.983416	0.994581	0.998404
$\|\varepsilon\|_{L^\infty}$	0.0645181	0.0351897	0.0181881	0.00926832	0.00473454
Order		0.874551	0.952158	0.972615	0.969084
$\|\mathbf{E}\|_2$	0.00694788	0.00345072	0.00170972	0.000849323	0.000423064
Order		1.009675	1.013137	1.009375	1.005437
$\|\mathbf{E}\|_{L^\infty}$	0.00722572	0.0038037	0.00190435	0.000945517	0.000470576
Order		0.925738	0.998105	1.010123	1.006676
$\|\mathbf{E}\|_{H^1}$	0.0495402	0.0246391	0.0120976	0.00595981	0.00295276
Order		1.007650	1.026229	1.021383	1.013202
$\|e\|_{L^2}$	0.040379	0.0203382	0.0101331	0.00504652	0.00251691
Order		0.989413	1.005116	1.005715	1.003635
$\|e\|_{L^\infty}$	0.0691807	0.0359907	0.0180811	0.00901139	0.00449888
Order		0.942745	0.993142	1.004661	1.002184

Table 2
Error and convergence rate of the second-order Gauge–Uzawa scheme in convective form with finite element $(\mathscr{P}^1, \mathscr{P}^2, \mathscr{P}^1)$ for $(\rho, \mathbf{u}, p)$, $\mu = 1$ and $\tau = h$

$\tau = h$	1/8	1/16	1/32	1/64	1/128
$\|\varepsilon\|_{L^2}$	0.00536121	0.00153932	0.000409795	0.000105529	2.67632e−05
Order		1.800266	1.909319	1.957263	1.979317
$\|\varepsilon\|_{L^\infty}$	0.00671147	0.00184529	0.000480763	0.000122597	3.0921e−05
Order		1.862781	1.940450	1.971402	1.987265
$\|\mathbf{E}\|_2$	0.000547451	0.000151833	4.01149e−05	1.02998e−05	2.60881e−06
Order		1.850245	1.920275	1.961522	1.981153
$\|\mathbf{E}\|_{L^\infty}$	0.000591473	0.000162425	4.53672e−05	1.19136e−05	3.03836e−06
Order		1.864539	1.840052	1.929040	1.971245
$\|\mathbf{E}\|_{H^1}$	0.00350691	0.00102363	0.000279096	7.2713e−05	1.85415e−05
Order		1.776506	1.874861	1.940476	1.971455
$\|e\|_{L^2}$	0.00511148	0.00130559	0.000329946	8.29264e−05	2.07863e−05
Order		1.969039	1.984400	1.992326	1.996199
$\|e\|_{L^\infty}$	0.00864952	0.00247663	0.000705502	0.000197117	5.43216e−05
Order		1.804242	1.811656	1.839598	1.859454

Table 3
Physical parameters for Example 2

Parameter	Air	Water	Unit (MKS)
Density (ρ)	1.161	995.65	kg/m^3
Viscosity (μ)	0.0000186	0.0007977	kg/ms

4.2. Example 2: An air bubble rising in water

This example has been simulated by a number of authors in a two dimensional rectangular domain (cf. [8]), although the situation can not be realized in an experimental setting, as well as in a cylinder (cf. [1]). To com-
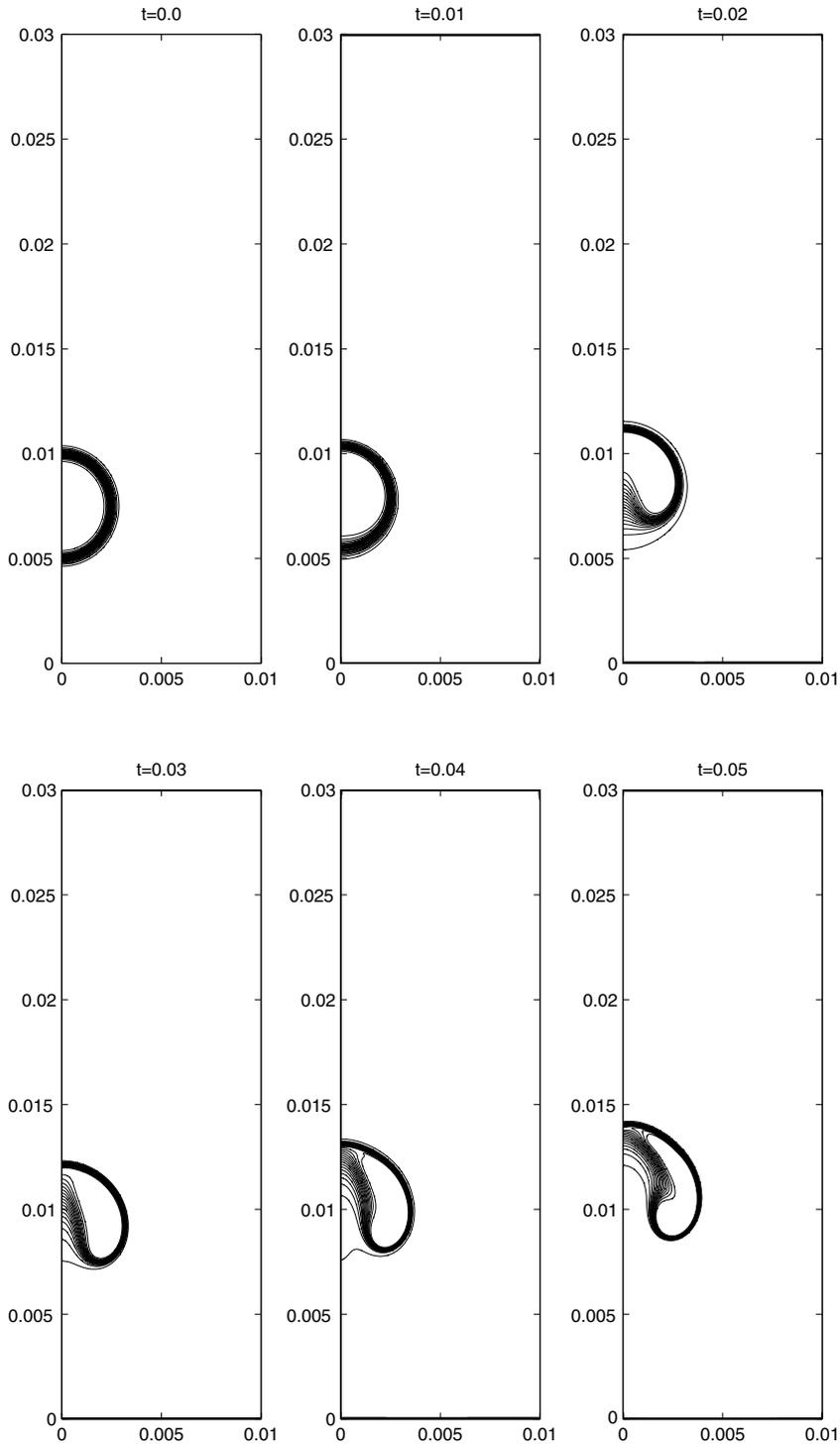
Fig. 1. Air bubble rises in a rectangular domain filled with water – I.

pare with the available numerical simulations, we carried out simulations in both situations using the FEM specified before with the Gauge–Uzawa scheme in convective form. The physical parameters we used are listed in Table 3. They are the same as in [8]. The finite element space $(\mathscr{P}^1, \mathscr{P}^2, \mathscr{P}^1)$ for $(\rho, \mathbf{u}, p)$ is used for both simulation with $h = 0.01/256$ m and $\tau = 1/10{,}000$ s.

Since the air and water have different viscosities, we replace the viscous term $-\mu \Delta \mathbf{u}$ by $-\nabla \cdot (\mu(\rho) \nabla \mathbf{u})$, so in the FEM implementation, the bilinear form $\mu \langle \nabla \mathbf{u}, \nabla \mathbf{v} \rangle$ in (2.19) is replaced by $\langle \mu(\rho) \nabla \mathbf{u}, \nabla \mathbf{v} \rangle$. We approximate the initial discontinuous density at the air–water interface by

$$\rho(\mathbf{x}, 0) = \rho_{\text{air}} + \left(\frac{\rho_{\text{water}} - \rho_{\text{air}}}{2} \right) \times \left(1 + \tanh \left(\frac{d - 0.0025}{0.00025} \right) \right), \tag{4.9}$$

where d is the distance from the center of the bubble to the point. The discontinuity for the viscosity is handled in a similar fashion. Gravity is accounted for via the force term $\frac{\mathbf{f}}{\rho} = [0, -9.80665 \text{ kg/m}^2]^{\text{T}}$. The initial condition for the velocity is set to be zero.

We first computed the problem in a rectangle of size $[0, 0.02 \text{ m}] \times [0, 0.03 \text{ m}]$ with an air bubble of radius 0.25 cm initially in the lower middle of the rectangle filled with water. We assume that the flow remains to be symmetric so the computational domain is reduced by half. Snapshots of the air bubble at nine different times from 0 to 0.8 s are displayed in Figs. 1 and 2. These results are essentially the same as those reported in [8]. The slight difference between our results and theirs may be due to the fact in their computation, an artificial homogeneous Neumann boundary condition was applied to the density, while in our computation, no boundary condition is enforced on the density since the inflow boundary $\Gamma_{\mathbf{u}}$ is empty.

Next, we consider a physically realistic situation, namely, the rise of an air bubble of radius 0.25 cm initially in the lower middle axis of a cylinder of radius 1 cm and hight 3 cm filled with water. We assume that the flow remains to be axisymmetric so the computational domain is $[0, 0.01 \text{ m}] \times [0, 0.03 \text{ m}]$. Snapshots of the air bubble at twenty different times from 0 to 0.19 s are displayed in Figs. 3–6. It can be noted that the bubble in the cylinder evolves quite differently form the rectangular case. We also observe that the Gauge–Uzawa algorithm is even robust as the bubble goes through a topological change around $t = 0.1$ s when a large part of the bub-
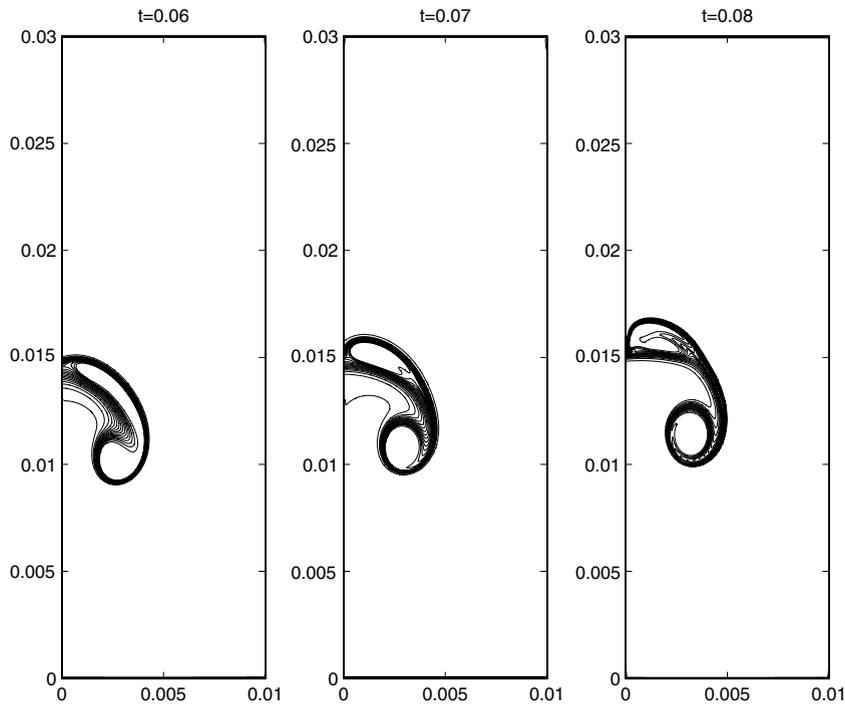
Fig. 2. Air bubble rises in a rectangular domain filled with water – II.
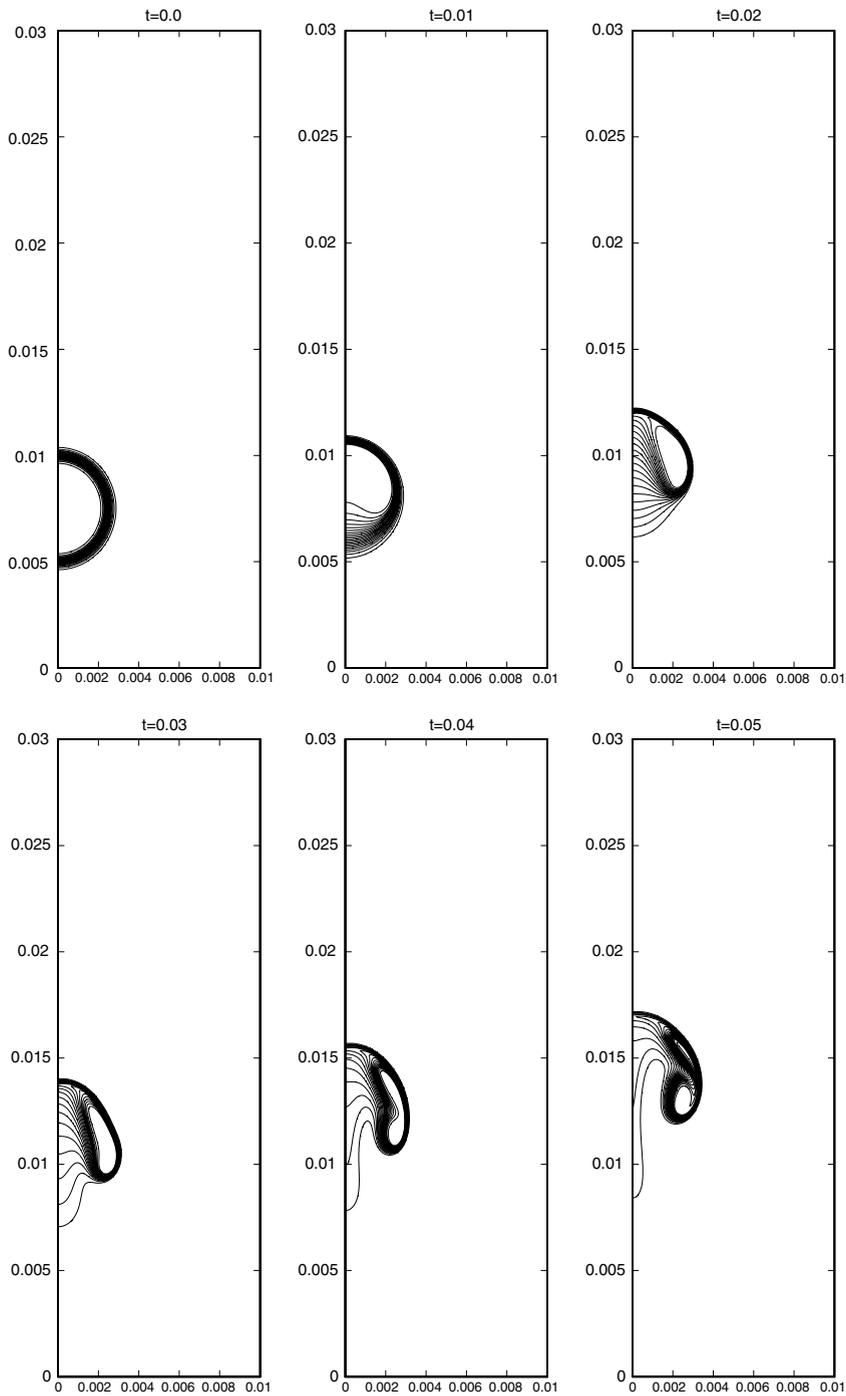
Fig. 3. Air bubble rising in a cylinder filled with water – I.

ble is detached from the axis. We note that this detachment may be due to the lack of surface tension in the governing equations; since the main purpose of the paper is to develop efficient and stable algorithms for flows with variable density, we will leave the surface tension effect on this problem to a future study. Finally, we note that our results at early times are qualitatively consistent with those presented in [1] where the results were computed with a constant viscosity of the water and only up to $t = 0.022$ s.
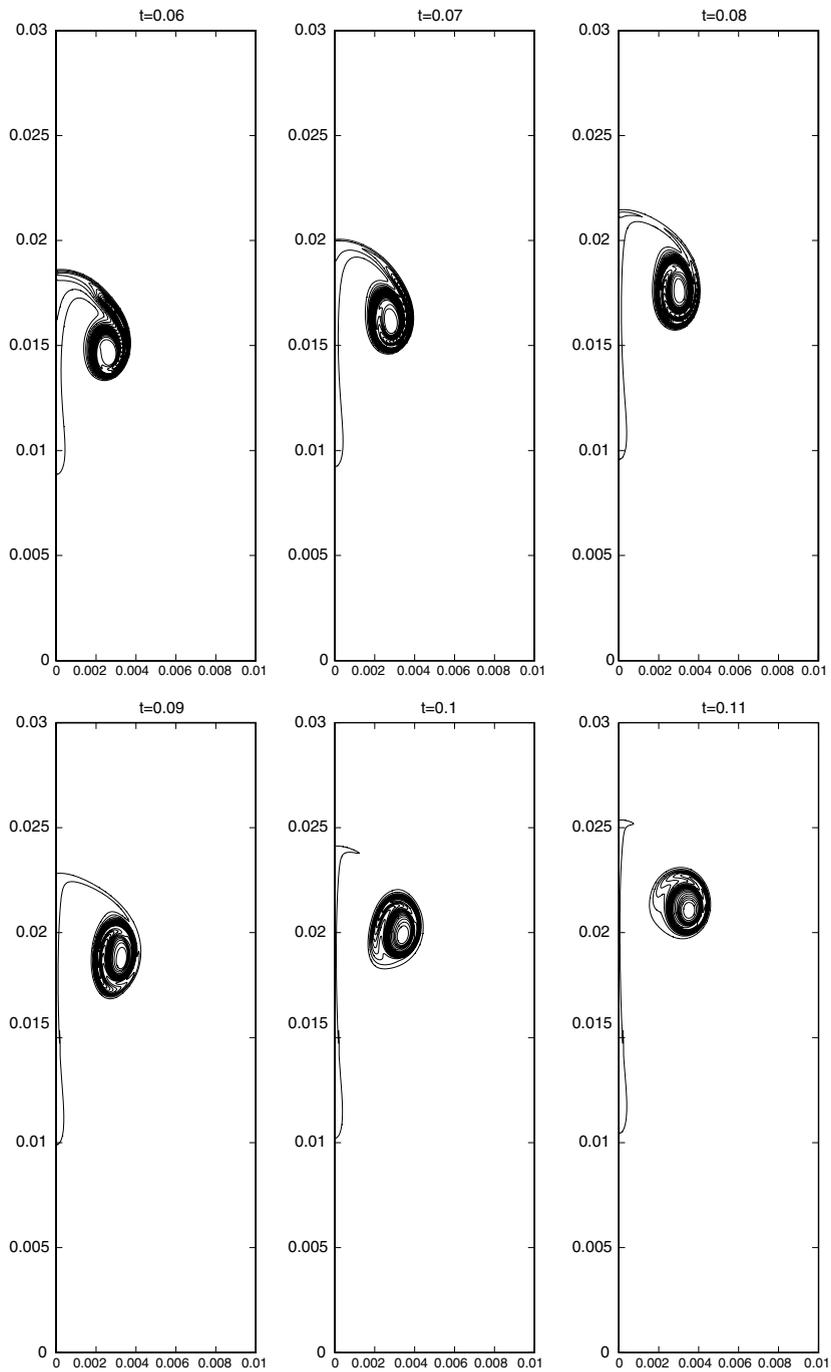
Fig. 4. Air bubble rising in a cylinder filled with water – II.

5. Concluding remarks

We presented in this paper two new Gauge–Uzawa schemes for incompressible flows with variable density and proved that the first-order versions of both schemes, in their semi-discretized form, are unconditionally stable. The first scheme is based on the conserved form and its stability proof can be readily carried over
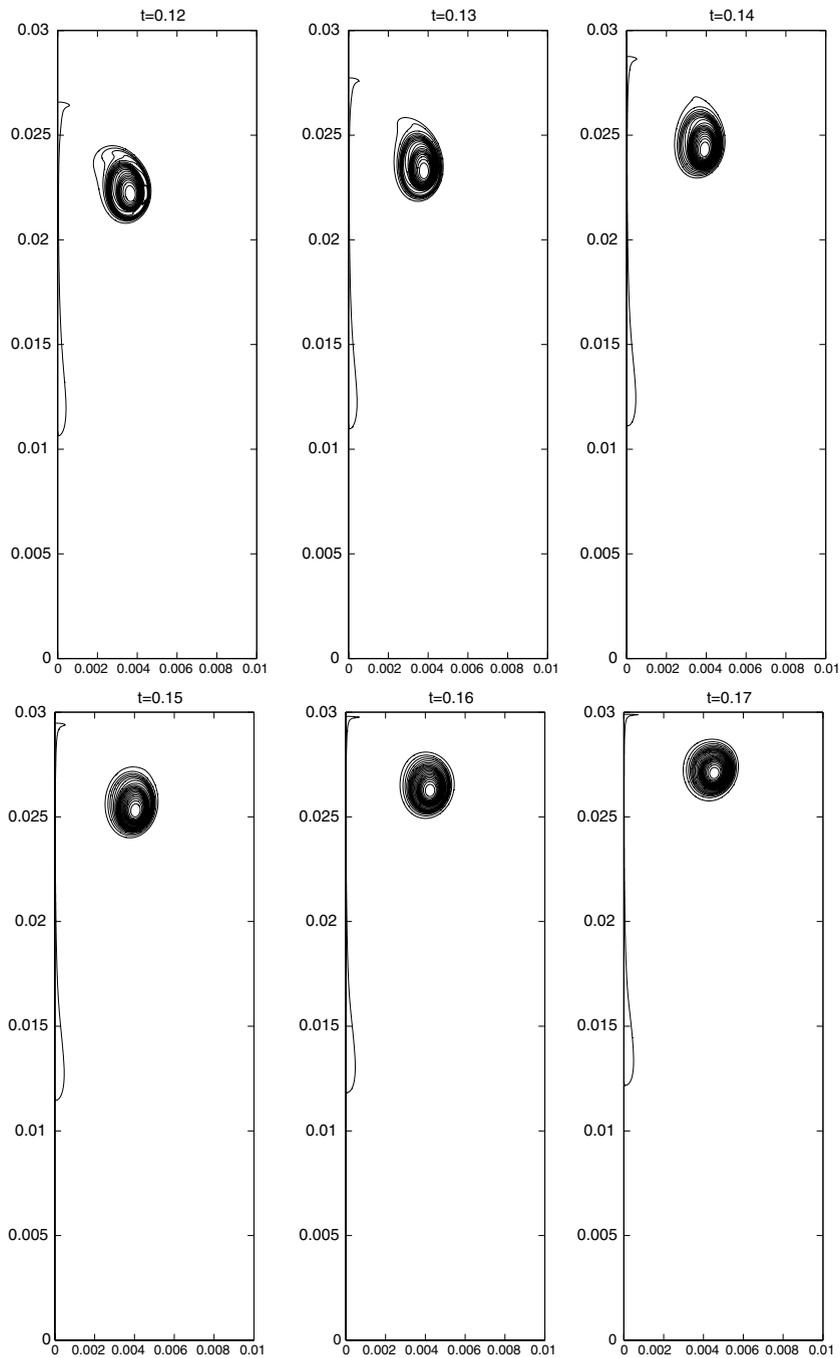
Fig. 5. Air bubble rising in a cylinder filled with water – III.

to its finite element discretization without using the incompressibility condition. The second scheme is based on a convective form which is computationally more efficient but its stability proof relies on the incompressibility condition. As opposed to the incremental projection scheme introduced in [6], our schemes only involve one projection step so they are more attractive computationally and easier to analyze as well.
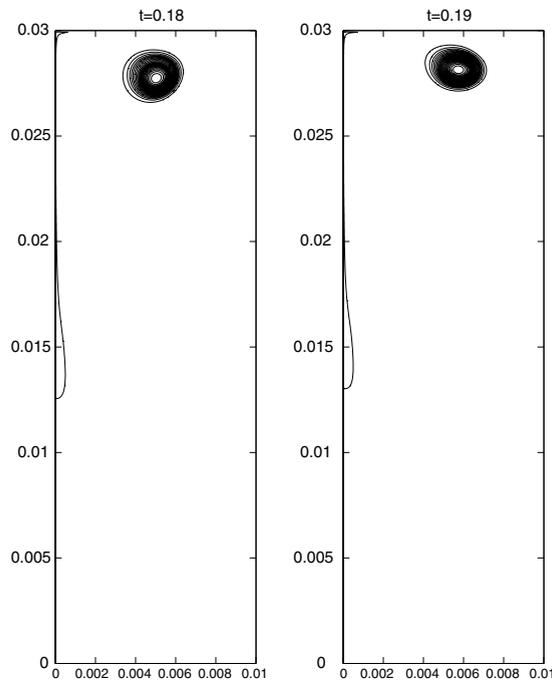
Fig. 6. Air bubble rising in a cylinder filled with water – IV.

We presented numerical evidence that first-order (resp. second-order) versions of the two schemes lead to first-order (resp. second-order) convergence rate for all variables. We also presented numerical simulations of air bubble rising in a cylinder filled with water as well as in a rectangle filled with water. Our numerical results are consistent with those available in the literature.

Our stability analysis and numerical experiments indicate that the new schemes are well suited for numerical simulation of incompressible flows with variable density.

References

[1] Ann S. Almgren, John B. Bell, Phillip Colella, Louis H. Howell, Michael L. Welcome, A conservative adaptive projection method for the variable density incompressible Navier–Stokes equations, J. Comput. Phys. 142 (1) (1998) 1–46.

[2] A.J. Chorin, Numerical solution of the Navier–Stokes equations, Math. Comput. 22 (1968) 745–762.

[3] E. Weinan, Jian-Guo Liu, Gauge method for viscous incompressible flows, Commun. Math. Sci. 1 (2) (2003) 317–332.

[4] Alexandre Ern, Jean-Luc Guermond, Theory and practice of finite elementsApplied Mathematical Sciences, vol. 159, Springer, New York, 2004.

[5] J.L. Guermond, P. Minev, J. Shen, An overview of projection methods for incompressible flows. Comput. Methods Appl. Mech. Eng., in press, doi:10.1016/j.cma.2005.10.010.

[6] J.-L. Guermond, L. Quartapelle, A projection FEM for variable density incompressible flows, J. Comput. Phys. 165 (1) (2000) 167–188.

[7] Claes Johnson, Numerical Solution of Partial Differential Equations by the Finite Element Method, Cambridge University Press, Cambridge, 1987.

[8] Hans Johnston, Jian-Guo Liu, Finite difference schemes for incompressible flow based on local pressure boundary conditions, J. Comput. Phys. 180 (1) (2002) 120–154.

[9] Pierre-Louis Lions. Mathematical topics in fluid mechanics. Vol. 1, volume 3 of Oxford Lecture Series in Mathematics and its Applications. The Clarendon Press Oxford University Press, New York, 1996. Incompressible models, Oxford Science Publications.

[10] R. Nochetto, J.-H. Pyo, The Gauge–Uzawa finite element method part I: the Navier–Stokes equations, SIAM J. Numer. Anal. 43 (2005) 1043–1068.

[11] R. Nochetto, J.-H. Pyo, The Gauge–Uzawa finite element method part II: Boussinesq equations. Math. Models Methods Appl. Sci., to appear.

[12] J.-H. Pyo, The Gauge–Uzawa and related projection finite element methods for the evolution Navier–Stokes equations. Ph.D Dissertation, 2002.

[13] J.-H. Pyo, Jie Shen, Normal mode analysis of second-order projection methods for incompressible flows, Discrete Contin. Dyn. Syst. Ser. B 5 (3) (2005) 817–840.

[14] R. Temam, Sur l'approximation de la solution des equations de Navier–Stokes par la methode des pas fractionnaires. II, Arch. Rational Mech. Anal. 33 (1969) 377–385.